Fatigue testing methods of carbon/epoxy composites

Zheng He, Xuan Gu [a,*], Xiaoyu Sun, Jianxin Teng, Yingshu Pang

College of Aerospace and Civil Engineering, Harbin Engineering University, Harbin 150001 China

[a] guxuan@hrbeu.edu.cn

Abstract

An experimental study is described in this paper dealing with the tension–tension fatigue and failure mechanism of 3D MWK composites with different fiber architectures and material sizes. Macroscopic fracture morphology and SEM micrographs are examined to understand the fatigue damage and failure mechanism. The results show the fatigue properties and failure mechanism of composites can be affected significantly by the fiber architecture and material size. The fatigue life of material A(0°/0°/0°/0°) with small fiber orientation angle is significantly longer than that of material B(+45°/−45°/+45°/−45°). For material A, the fatigue properties of the long composite are better than that of the short one. It is 0° fiber bundles fracture under fatigue stress which cause the material failure and the long composite provides more space for the formation and propagation of local fatigue micro-cracks. However, for material B, the short composites have better fatigue properties. Moreover, the materials show typical ±45° zigzag fatigue fracture and obvious shear behavior. The fatigue cracks for the long composite can be spread more quickly along the fiber/matrix interface due to the fiber bundles realignment.

Keywords

A. Polymer–matrix composites (PMCs); B. Fatigue; B. Mechanical properties; D. Electron microscopy; E. Knitting.

1. Introduction

Three-Dimensional (3D) composites have been developed recently by the advanced textile techniques such as weaving, knitting, braiding and stitching in an attempt to produce near-net-shape preforms and overcome many of the problems with the manufacturing and mechanical properties of conventional 2D laminates. In particular, 3D multi-axial warp knitted (MWK) approach is well suited to the rapid manufacture of components to overcome damage tolerance problem and weak strength in the thickness direction. The most attractive feature of this composites is the fabrics perform consist of unidirectional plies with no crimp arranged in a number of different orientations relative to the fabric production direction; the individual plies are kept together by stitching yarns using warp knitting process technology. In recent years, the use of 3D MWK composites is growing rapidly in aircraft, automobiles, marines, wind turbine blades and other complex structural components[1-4].

It is valuable to study the fatigue behavior and failure mechanism of 3D multi-axial warp knitted composite because of its wide potential applications in engineering, especially when they are used in aerospace structures. This paper presents an experimental study on the tensile fatigue properties of 3D MWK composites with different fiber architecture and material size. The damage and fracture morphology of the composites after failure are observed from the macroscopic and microscopic views and the fatigue failure mechanism is demonstrated. Furthermore, the influences of the fiber architecture, the material size on the fatigue properties and failure mechanism of composites are also

analyzed. The aim of our study is to assist in establishing the database and providing an experimental basis for the potential applications of 3D MWK composites.

2. Experimental

3D MWK performs are made from layers of non-crimp fabric(made with unidirectional tows) stacked in the required orientations and then bound together with binder yarns inserted in the through-thickness direction by warp knitting needles. Fig. 1 shows the schematic of 3D MWK perform manufacturing. In this study, E-glass fiber bundles are used for unidirectional reinforcing in 0°, 45° or −45° directions while polyester fiber bundles are used for knitted linking and two kinds of structure with different fiber orientation A[0°/0°/0°/0°], B[+45°/−45°/+45°/−45°] are manufactured. Twelve fiber layers with non-crimp are used in the 3D MWK composites and the fiber volume fraction is 60%. Fig. 2 shows the photographs of the face and the back of two types of orientation preforms (0° and +45°). 3D MWK performs are injected into the epoxy resins by the Vacuum Assisted Resin Transfer Molding (VARTM) process and then consolidated to produce the 3D MWK composites. The composites are then cut as dog-bone shape using a water-lubricated diamond saw for static tensile and fatigue tests. The dimensions of the long specimens are 200 mm(length) × 9 mm(width) × 2.5 mm(thickness) with the clear distance between grips 80 mm; the dimensions of the short specimens are 120 mm(length) × 9 mm(width) × 2.5 mm(thickness) with the clear distance between grips 10 mm. Here, the notations of the long and short specimens for material A and B, are AL, AS and BL, BS respectively. Fig. 3 shows that the photographs of specimens BL and BS.

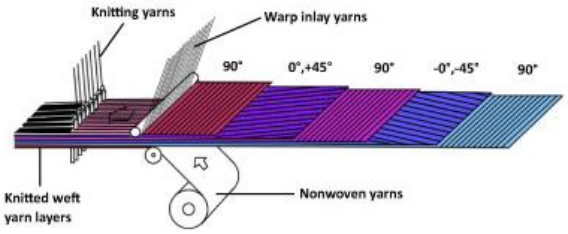

Fig. 1. 3D multi-axial warp knitted system.

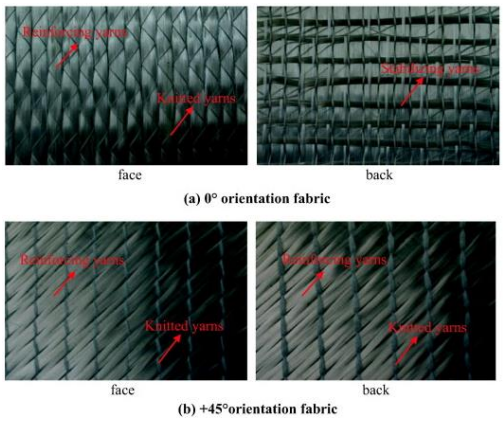

Fig. 2. Photographs of 3D MWK preforms.

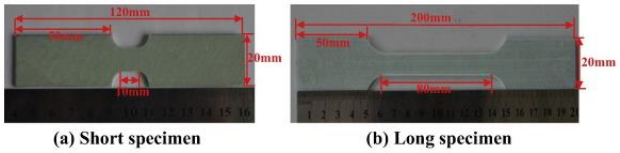

Fig. 3. The fatigue specimen.

A hydraulic Instron 8874K4979 fatigue machine with a load cell of 25 kN was adopted for fatigue investigation. With refer to ASTM D3479/D3479M standard, fatigue testing was performed under constant stress amplitude, an alternating sinusoidal wave-form tensile–tensile loading. The stress ratio, $R(\sigma\min/\sigma\max)$, of the minimum load (σmin) to the maximum load (σmax) in the cycle was kept

constant to be 0.1. Fatigue tests were carried out at normalized applied stress *S*max(σmax/σult) (0.8, 0.7, 0.55, 0.4) in order to have a complete characterization. In order to reduce self-generated heating in the specimen, the frequency of the stress cycle was 5 Hz at ambient temperature. This frequency was selected after verifying that the maximum temperature reached by the specimen during the test did not exceed 25 °C. The fatigue experimental procedure is shown schematically in Fig. 4.

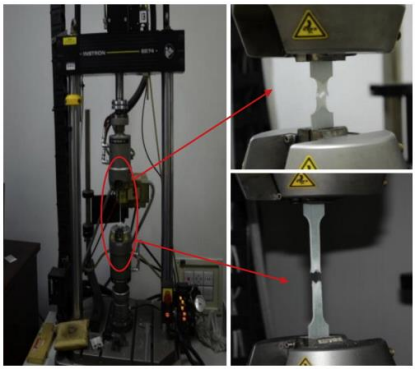

Fig. 4. The fatigue experiment procedure.

3. Results and discussion

Fig. 5 gives the tensile stress vs. strain curves for two types of composites. It can be found that the fiber architecture has a significant effect on the stress–strain curves. For material A, it can be seen that the curve shows obvious linear elastic feature up to failure and the material exhibits brittle fracture characteristics. This is due to the fact that there is no crimp for the fiber bundles inside the material, and fiber bundles act as the main load-bearing object which can bear load until the failure occurred. However, the curve for material B shows significant nonlinear transition and exhibits an obvious plastic platform which attributes to different failure mechanisms. The ±45° fiber/matrix interfaces are the main load-bearing objects, the degradation of the matrix between the fibers increases gradually which exhibits progressive loss of stiffness. From the stress vs. strain curves, the ultimate strength (σult) of the composites can be obtained, that is: σult-A for material A is 753.3 MPa and σult-B for material B is 152.0 MPa.

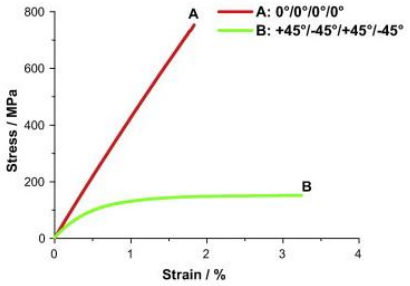

Fig. 5. The tensile stress vs. strain curves.

Fig. 6(a) shows the results of the maximum fatigue stress plotted against the fatigue life for 3D MWK composites with different fiber architecture. It can be found that the fatigue performance of material B is lower than that of material A. In fact, the low fatigue performance of material B is related to their lower ultimate stress found in the static tests, which is caused by the absence of the fiber bundles that can efficiently bear the fatigue load in the 0° direction. Fig. 6(b) shows the comparison of the fatigue properties based on the relationship between the normalized fatigue stress and fatigue life. It can be found that the fiber architecture and material size have significant influence on the fatigue life of composites. For the composites with the same tested length, the fatigue life of material A is always longer than that of material B over the entire range of stress investigated.

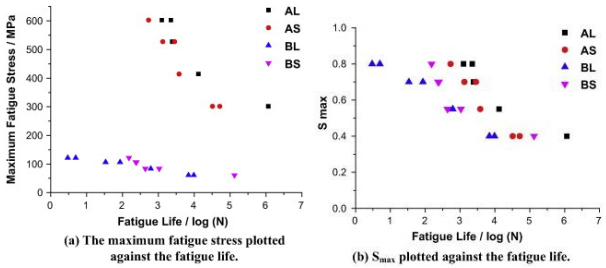

Fig. 6. The fatigue performance of 3D MWK composites.

Power-law regression equations (*S*max = *a* * (log N)b) are determined for the evaluation of fatigue test data. As shown in Fig. 7(a), for material A, no matter long samples or the short one, the power function can be fitted the experiment plots very well, it is clear that in all the fatigue zone, for the same normalized applied stress *S*max, the fatigue life of long samples is obviously bigger than the short one. However, for material B (Fig. 7(b)), the power function can be simulated very well for the short sample, but totally not for the long samples. And the experimental data shows a relatively small scatter and can be well described with the linear function for the long samples, which are consistent with those from other literatures[5-6]. Comparing the two fitted curves, it can be seen further that the fatigue life of the short composites is longer than that of the long composites in the entire fatigue zone.

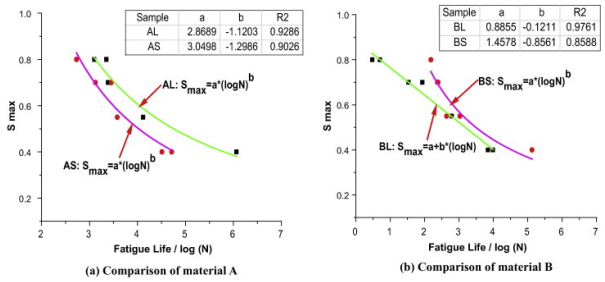

Fig. 7. The fitted fatigue curves of *S*max vs. log *N*.

In order to investigate the type of damage and failure mechanism, the morphology of fractures is observed by photos and scanning electron microscope (JSM 7500F) from the macroscopic and microscopic views. Fig. 8 shows the typical fatigue failure morphology of material under the same *S*max level (0.7). It is found that the damage and failure morphology are different from the fiber architecture of composites.

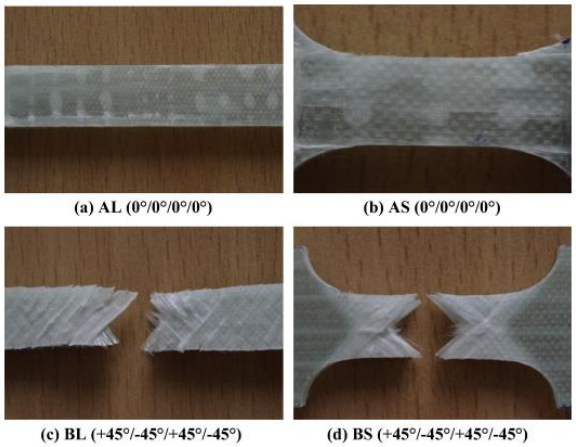

Fig. 8. The fatigue fracture photographs (*S*max = 0.7).

By SEM observations, from Fig. 9(a), the matrix is cracked and the fatigue cracks extend along both directions. At the same time, the 0° fibers are curled and fractured inside the material where the splits exist (Fig. 9(b)). So, when the fatigue stress is applied on material A, it is the 0° fibers that act as the main load-bearing object.

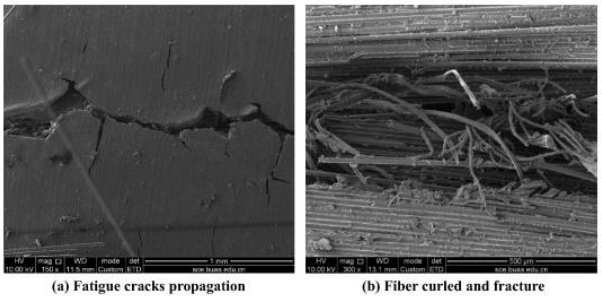

Fig. 9. The SEM photographs of material A. (*S*max = 0.7).

From Fig. 10(a), SEM observations show that the fatigue cracks formed on the edge of the materials and extended to the interior at 45° angle. At the same time, although the binding yarns boost the separation resistance between layers, the delamination fracture can be clearly observed from the fracture cross-section (Fig. 10(b)).

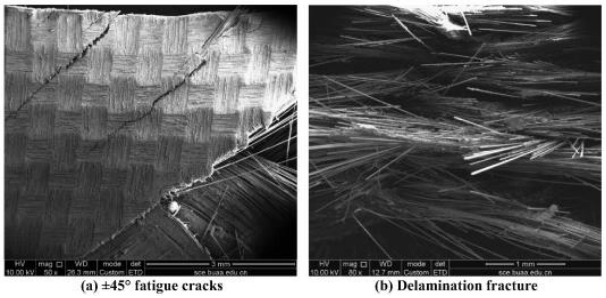

Fig. 10. The SEM photographs of material B. (*S*max = 0.7).

Fig. 11 shows the fatigue fracture photographs of material A with different material sizes at vary stress levels. It can be observed that the fatigue damage extent increases significantly with the increase of the stress level for both long and short specimens. This is due to the fact that at higher fatigue stress level, more fatigue cracks are stimulated to occur inside the material in order to relax the stress concentration. SEM observations show that the materials with long and short gauge length have similar fatigue damage. From Figs. 12(a) and 13(a), some 0° fibers are fractured evenly due to tensile fatigue normal stress and some are fractured in shear due to shear stress. From Figs. 12(b) and 13(b), it can be found that the matrix cracks, fiber/matrix interface are debonded and the fibers curled under the fatigue loads. However, for the long specimens AL, more space for the generation and extension of local fatigue cracks, which show a better fatigue life. While for the short specimens AS, the stress concentration is increased significantly due to limited space, which improve the possibility for the local destruction and shows bad fatigue life.

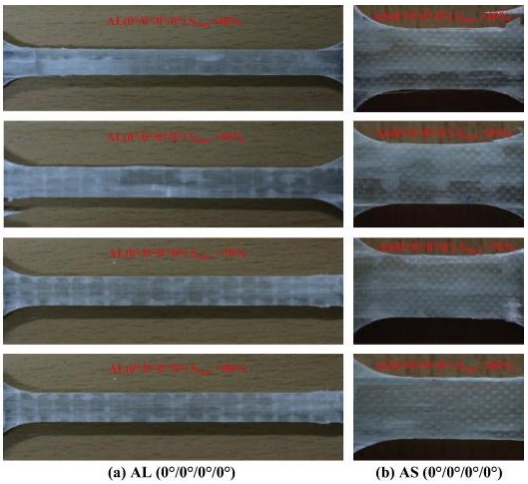

Fig. 11. The fatigue fracture photographs of material A at different stress levels.

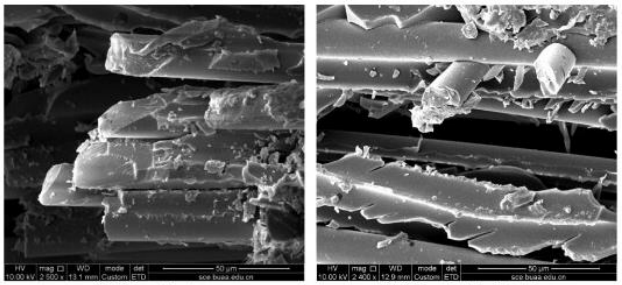

(a) Fibers fracture (b) Fiber/matrix interface

Fig. 12. The SEM photographs of specimen AL.

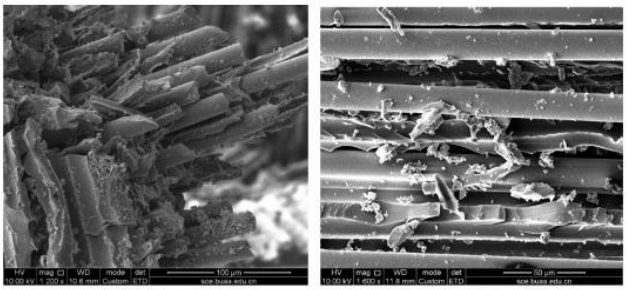

(a) Fibers fracture (b) Fiber/matrix interface

Fig. 13. The SEM photographs of specimen AS.

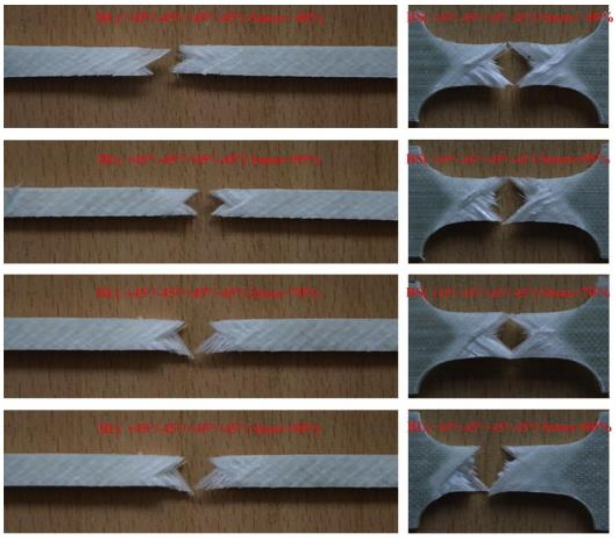

(a) BL (+45°/-45°/+45°/-45°) (b) BS (+45°/-45°/+45°/-45°)

Fig. 14. The fatigue fracture of material B at different stress levels.

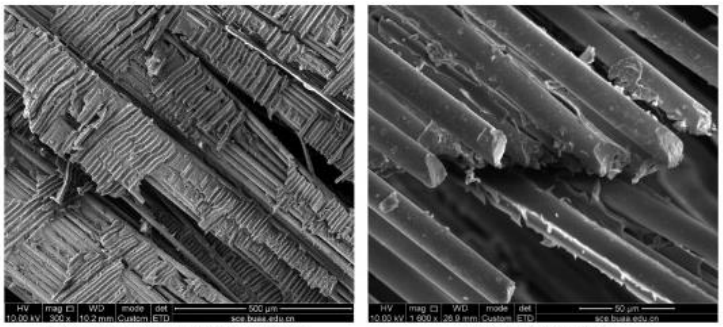

(a) Matrix crack and fibers realign (b) Fibers tearing

Fig. 15. The SEM photographs of specimen BL.

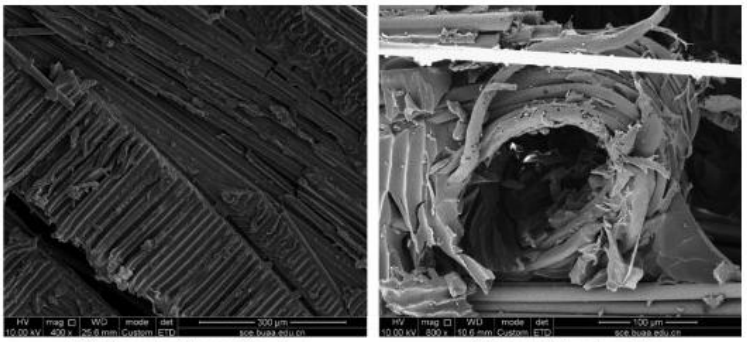

(a) Fibers tearing and fracture (b) Nest of fiber bundles

Fig. 16. The SEM photographs of specimen BS. (*S*max = 0.7).

Fig. 14 shows the fatigue fracture photographs of material B with different material size at vary stress levels. It can be seen that all the materials show typical ±45° zigzag fatigue fracture. The whitening matrix cracking damage and the fibers realign phenomenon can be obviously observed. For material B, it is ±45° fiber/matrix interface dominates the failure of material. Failure will occur when local crack grows unstably after it reaches a critical length by fatigue. So, for the long specimen BL, the fiber bundles realign themselves and form a smaller angle between the fiber orientation and fatigue load, the fatigue cracks can be extended more quickly along the fiber/matrix interface, which shows the short fatigue life. From Fig. 15(a) and (b), further SEM observations show that the matrix is cracked, the fibers are realigned and torn obviously. For the short specimen BS, it is more difficult for the ±45° fibers to realign due to more limited space and more fatigue cycles are needed for the fatigue micro-cracks propagation along ±45° fiber/matrix interface. From Fig. 16(a), during the fatigue cracks grow along fiber/matrix interface, the matrix are cracked and many fibers are fractured transversely due to limited space, which hinders the fatigue cracks to spread. On the other hand, an interesting nest of fiber bundles can be observed, which can also diffuse the fatigue energy (Fig. 16(b)). This is mainly because the tensile–tensile fatigue stress is more likely to be concentrated around fiber bundles of the short specimens and the sudden fiber slacks in the limited space lead to the crimping of fiber bundles.

4. Conclution

The tension–tension fatigue properties of 3D MWK composites with different fiber architectures and material sizes are studied. The fatigue life of material A(0°/0°/0°/0°) is significantly longer than that of material B(+45°/−45°/+45°/−45°) due to its high tensile strength. Moreover, the fatigue life of the long composite (AL) is obvious longer than that of the short one (AS), because more micro-cracks can be propagated and the stress concentration is decreased significantly. However, for material B, the fatigue life of the long composite (BL) is always shorter than that of the short one (BS), due to the fact that the longer specimen is, the fibers are more likely to realign themselves.

Acknowledgements

This work is supported by the National Natural Science Foundation of China（No. 11602066） and the National Science Foundation of Heilongjiang Province of China (QC2015058 and 42400621-1-15047), the Fundamental Research Funds for the Central Universities.

References

[1] A.P. Mouritz, M.K. Bannister, P.J. Falzon, K.H. Leong Review of applications for advanced three-dimensional fibre textile composites Composites Part A, 30 (1999), pp. 1445–1461

[2] R. Kamiya, B.A. Cheeseman, P. Popper, T.W. Chou Some recent advances in the fabrication and design of three-dimensional textile preforms: a review Compos Sci Technol, 60 (2000), pp. 33–47

[3] K.H. Leong, S. Ramakrishna, Z.M. Huang, G.A. Bibo The potential of knitting for engineering composites – a review Composites: Part A, 31 (2000), pp. 197–220
[4] W. Hufenbach, R. Böhm, M. Thieme, A. Winkler, E. Mäder, J. Rausch Polypropylene/glass fibre 3D-textile reinforced composites for automotive applications Mater Des, 32 (2011), pp. 1468–1476
[5] K. Vallons, M. Zong, S.V. Lomov, I. Verpoest Carbon composites based on multi-axial multi-ply stitched preforms – Part 6. Fatigue behaviour at low loads: stiffness degradation and damage development Composites Part A, 38 (2007), pp. 1633–1645
[6] M.R. Satapathy, B.G. Vinayak, K. Jayaprakash, N.K. Naik Fatigue behavior of laminated composites with a circular hole under in-plane multiaxial loading Mater Des, 51 (2013), pp. 347–356